Molecular Porous Photosystems Tailored for Long-Term Photocatalytic CO2 Reduction

F. Wisser, M. Duguet, Q. Perrinet, A. Ghosh, M. Alves-Favaro, Y. Mohr, C. Lorentz, R. Palkovits, D. Farrusseng, C. Mellot-Draznieks, et al.

HAL Id: hal-02892502
https://hal.science/hal-02892502

Submitted on 31 Jul 2020

Molecular Porous Photosystems Tailored for Long-Term Photocatalytic CO₂ Reduction

Florian M. Wisser,*[a] Mathis Duguet,[b] Quentin Perrinet,[c] Ashta C. Ghosh,[a] Marcelo Alves-Favaro,[a,d] Yorck Mohr,[a] Chantal Lorentz,[a] Elsje Alessandra Quadrelli,[e] Regina Palkovits,[d] David Farrusseng,[a] Caroline Mellot-Draznieks,[b] Vincent de Waele,[c] and Jérôme Canivet[a]

Abstract: Herein, we report the molecular-level structuration of two full photosystems into conjugated porous organic polymers. The strategy of heterogenization gives rise to photosystems which are still fully active after 4 days of continuous illumination. Those materials catalyse the carbon dioxide photoreduction driven by visible light to produce up to three grams of formate per gram of catalyst. The covalent tethering of the two active sites into a single framework is shown to play a key role in the visible light activation of the catalyst. The unprecedented long-term efficiency arises from an optimal photoinduced electron transfer from the light harvesting moiety to the catalytic site as anticipated by quantum mechanical calculations and evidenced by *in-situ* ultrafast time-resolved spectroscopy.

Introduction

In the perspective of green fuel production, non-restrictive photochemical processes using visible light as sole energy source open the appealing opportunity of a very low carbon footprint. The visible light-driven photochemical reduction of carbon dioxide catalysed by molecularly-defined species, shows high activity at short reaction times.[1–3]

So far, improvements of photocatalytic systems have been focused almost exclusively on the catalyst side. Enhancement of lifetime and efficiency of molecular catalysts has been achieved by their single-site heterogenization within molecularly-defined porous solids.[2,4,5] In most of those photosystems, Ir- and Ru-based organometallic photosensitizers were used although they suffer from photodegradation under continuous illumination.[6,7] Consequently, the catalytic activity of most photosystems is slowed down or even completely lost within less than 12 hours.

In contrast, purely organic photosensitizers are much more stable as compared to their molecular noble-metal counterparts.[6] Especially, conjugated organic solids benefit from higher photochemical stability originating from additional molecular geometry constraints.[8–11] Initiated by the seminal work of Antonietti and co-workers using carbon nitride as both heterogeneous organic photosensitizer and catalyst for hydrogen evolution reaction published in 2009,[12] conjugated polymer photocatalysts are attracting a growing interest.[8,13–17] Key for their success is the tunability of the polymers' properties by copolymerization of tailored monomers for a careful control of light absorption or porosity.[8,10,18] Also, recently the use of porous organic polymers or poly aromatic frameworks as photosensitizers has been reported for CO₂ reduction into CO, using different transition metal-based catalysts.[16,19–22] However, long-term stability remains an important challenge,[16] as such photocatalysts still showed deactivation within typically less than 15 hours. In addition bottom-up approaches for the design of better performing heterogeneous photocatalysts are restricted as only little is known on the fundamental mechanisms occurring during light harvesting and activation of the catalysts.[23,24]

Here we report tailor-made three-dimensional porous polymers made from molecular organic photosensitizers in which we heterogenized an efficient molecular catalyst. As a proof of our all-in-one concept, two Rh-based fully heterogeneous catalytic systems achieve constant photoreduction of CO₂ into formate under visible light irradiation during at least four days of continuous illumination. This unprecedented long-term activity is achieved without any measurable degradation over time, achieving a total production of three grams of formate per gram of catalyst. The unique stability and activity arise from the perfect electronic interplay between the site-isolated species, caused by their regular interconnection on a molecular level in one framework. The ultrafast energy transfer from the photosensitizer to the catalyst has been assessed by *in-situ* ultrafast time-resolved spectroscopy and quantum mechanical calculations.

Results and Discussion

Our synthetic strategy here consists in integrating an active organometallic catalyst into a photosensitive porous organic matrix. We have chosen monomers based on photoactive perylene or pyrene cores to synthesize microporous macroligands[5,25,26] that consist of alternating photosensitizers and metal binding sites called hereafter **Pe**rylene-*alt*-**Bipy**ridine-**C**onjugated **M**icroporous **P**olymers (**PerBpyCMP**) and **Py**rene-*alt*-**Bipy**ridine-**CMP** (**PyBpyCMP**). Then the Cp*Rh catalytic synthon was coordinated to the different frameworks to obtain the heterogeneous photocatalysts

[a] Dr. F. M. Wisser, Dr. A. C. Ghosh, Mr. M. Alves-Favaro, Mr. Y. Mohr, Ms. C. Lorentz, Dr. D. Farrusseng, Dr. J. Canivet
Université de Lyon, Université Claude Bernard Lyon 1, CNRS, IRCELYON - UMR 5256, 2 Avenue Albert Einstein, 69626 Villeurbanne Cedex, France
E-mail: florian.wisser@ircelyon.univ-lyon1.fr

[b] Mr. M. Duguet, Dr. C. Mellot-Draznieks
Laboratoire de Chimie des Processus Biologiques (LCPB) Collège de France, PSL Research University, CNRS Sorbonne Université, 11 Place Marcelin Berthelot, 75231 Paris Cedex 05, France

[c] Mr. Q. Perrinet, Dr. V. de Waele
Univ. Lille, CNRS, UMR 8516, LASIR–Laboratoire de Spectrochimie Infrarouge et Raman, F-59000 Lille, France

[d] Mr. M. Alves-Favaro, Prof. Dr. R. Palkovits
Institut für Technische und Makromolekulare Chemie, RWTH Aachen University, Worringerweg 2, 52074 Aachen, Germany

[f] Dr. E. A. Quadrelli
Université de Lyon, Université Claude Bernard Lyon 1, CPE Lyon, CNRS, C2P2 - UMR 5265, 43 Bvd du 11 Novembre 1918, 69616 Villeurbanne, France

Cp*Rh@PyBpyCMP and **Cp*Rh@PerBpyCMP** (**Figure 1a**), following a well-established grafting procedure.[5]

Both catalysts, **Cp*Rh@PyBpyCMP** and **Cp*Rh@PerBpyCMP**, have a permanent porosity towards nitrogen at 77 K, with apparent surface areas of approximately 200 m²/g, as well as a high CO_2 uptake of up to 6 wt.-% (**Figure 1b, c**), a key feature for a high activity in the targeted catalysis.[27] Moreover, a good wettability of the catalysts with the reactions' solvent (here acetonitrile) is essential to have access to all active sites.[28] Vapour physisorption isotherms of acetonitrile reveal similar surface wettability and high degrees of pore-filling for the two solid catalysts (**Figure 1c**, **Table S1**), allowing also for direct comparison of their activities.

Complete copolymerization of bipyridine-based monomers with perylene and pyrene cores was confirmed by solid-state NMR spectroscopy. All materials are free of residual pinacolborane moieties in contrast to similar materials reported in literature, prepared in toluene instead of DMF (**Figure 1d**, **Figure S4** & **S5**).[29] From the quantitative ¹³C multiCP MAS NMR spectra, a catalyst loading in both materials of approx. 6 mol-% is obtained (in line with ICP analysis, see **Table S2**). Thus, one catalytic active site is surrounded by approx. 20 chromophores, ensuring sufficient photosensitization.

Solid-state UV-Vis spectroscopy demonstrates that the bandgap can be controlled by changing the chromophore. As expected from the properties of molecular building units, **Cp*Rh@PerBpyCMP** shows a smaller bandgap than that of **Cp*Rh@PyBpyCMP,** *i.e.* 1.98 ± 0.10 eV *vs* 2.35 ± 0.05 eV, as a result of the larger aromatic system of perylene (**Figure 1e**).

To gain insight into the influence of the nature of the chromophores on their electronic structure and the corresponding molecular frontier orbitals, DFT-calculations were performed on molecular clusters.[10,30–32] Here we anticipated that the molecular frontier orbitals of the constitutive molecular unit are representative of those of the solids. Calculations on the Rh-free clusters (**Figure 2a**) reveal that the frontier orbitals of [py₂(bpy)] (molecular cluster of **PyBpyCMP**) are fully localized on both pyrene and bipyridine moieties, as a result of the expected hybridization of π-orbitals.[33] Remarkably, frontier orbitals are mainly found on the perylene chromophore in [per₂(bpy)] (molecular cluster of **PerBpyCMP**). The HOMO-LUMO gaps of [py₂(bpy)] and [per₂(bpy)] are of 3.43 and 2.92 eV, respectively (**Figure S27**).

In contrast, the presence of the Rh-metal center significantly reduces the HOMO-LUMO gap of both complexes down to 3.11 eV for [py₂(bpy)]Cp*RhCl₂ and 2.64 eV for [per₂(bpy)]Cp*RhCl₂. Interestingly, the LUMOs of both Rh-clusters exhibit electronic densities localized near the Rh-metal centre and the bipyridine moiety, while the HOMOs are localized exclusively on the chromophores (**Figure 2b**). Unlike
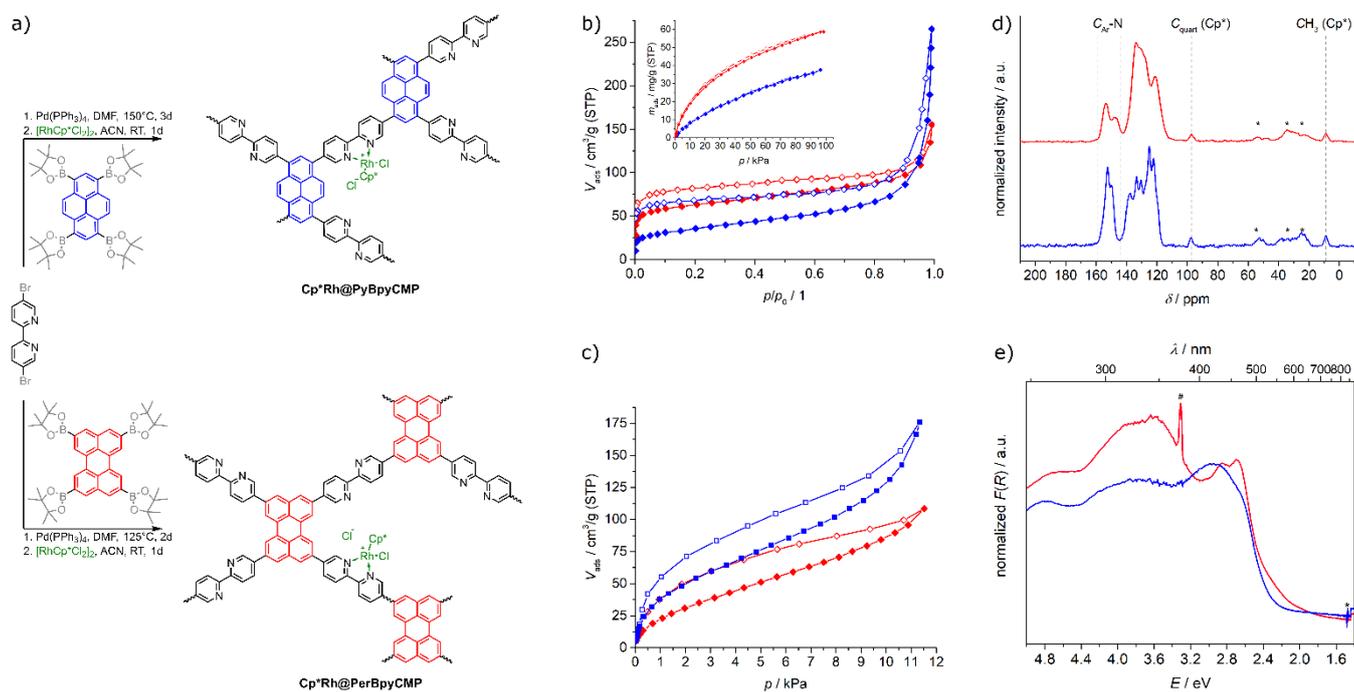

Figure 1. **a)** Scheme of the stepwise synthesis of completely heterogeneous photocatalysts: **1.** Pd-catalyzed Suzuki-polycondensation of the photoactive core containing microporous macroligand, *viz.* pyrene core in **Cp*Rh@PyBpyCMP** (blue) and perylene core in **Cp*Rh@PerBpyCMP** (red). **2.** Rh infiltration to integrate the Rh-based photocatalytic site [RhCp*Cl]Cl (green). **b)** N₂ physisorption isotherms measured at 77 K and CO₂ physisorption isotherms measured at 273 K (inset) of **Cp*Rh@PyBpyCMP** (blue) and **Cp*Rh@PerBpyCMP** (red, closed symbols represent adsorption, open symbols desorption), **c)** acetonitrile vapour physisorption isotherms measured at 298 K of **Cp*Rh@PyBpyCMP** (blue) and **Cp*Rh@PerBpyCMP** (red, closed symbols represent adsorption, open symbols desorption), **d)** ¹³C multiCP MAS NMR spectra of **Cp*Rh@PyBpyCMP** (blue) and **Cp*Rh@PerBpyCMP** (red, * denote spinning sidebands) and **e)** solid state UV-Vis spectra of **Cp*Rh@PyBpyCMP** (blue) and **Cp*Rh@PerBpyCMP** (red, #,* denote signals from the experimental setup).
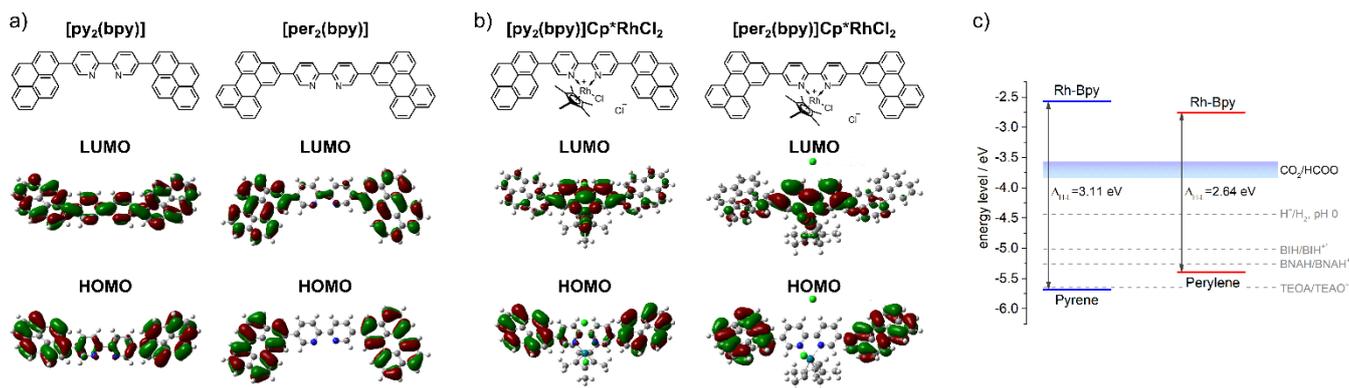
Figure 2. a) HOMO and LUMO surfaces calculated for [py₂(bpy)] and [per₂(bpy)] (model clusters of metal-free **PyBpyCMP** and **PerBpyCMP** respectively) at the *B3LYP/6-311++g(d,p)* level of theory; **b)** HOMO and LUMO surfaces calculated for [py₂(bpy)]Cp*RhCl₂ and [per₂(bpy)]Cp*RhCl₂ (metallated model clusters for **Cp*Rh@PyBpyCMP** and **Cp*Rh@PerBpyCMP**, respectively) at *B3LYP/6-311++g(d,p)/LanL2DZ* level of theory. Color code: grey: C, white: H, blue: N, light green: Cl and turquoise: Rh; **c)** Diagram of HOMO and LUMO energy levels of [py₂(bpy)]Cp*RhCl₂ (blue) and [per₂(bpy)]Cp*RhCl₂ (red) using ionization potentials to align HOMOs, together with redox potentials in eV for formate production (pH range: 0 to 9; estimated pH of the reaction mixture), hydrogen evolution reaction and sacrificial electron donors BIH, BNAH and TEOA. Please note that the calculated LUMO position for [py₂(bpy)]Cp*RhCl₂ is in line with the experimentally accessible reduction potential of [py₂(bpy)]Cp*RhCl₂ measured in acetonitrile by cyclic voltammetry (**Table S7, Figure S34**).

metal-free clusters, the Rh coordination triggers a chromophore-to-bipyridine controlled HOMO-LUMO transition.[33] Thus, after, light absorption and relaxation processes, the photo-excited electron should be centred next to the catalytically active Rh moiety representing an efficient charge separation. This charge separation close to the active site is an important feature in the design of supramolecular photocatalysts to drive the photochemical reduction reaction.[1,34,35]

Moreover, knowledge of HOMO and LUMO positions with respect to the redox potential of the half-reactions under study gives insight into the thermodynamic driving forces.[36] The calculations on [py₂(bpy)]Cp*RhCl₂ and [per₂(bpy)]Cp*RhCl₂ show that the LUMO energy levels are well above the potential required for CO_2-to-formate reduction. Even under basic conditions, the driving force for CO_2 reduction is considerable (> 0.8 eV) for both catalysts (**Figure 2c**). However, the driving force for the oxidation of the sacrificial electron donor, the second half-reaction occurring, strongly depends on the nature of the chromophore. The energy level of the involved HOMO are found at higher energy for [per₂(bpy)]Cp*RhCl₂. This higher energy level is attributed to the better delocalization of the π-system.

Next, we experimentally evaluated the photocatalytic activities of the two fully heterogeneous photosystems **Cp*Rh@PyBpyCMP** and **Cp*Rh@PerBpyCMP** in CO_2 reduction. The experiments were performed in a CO_2 saturated acetonitrile-triethanolamine mixture using 1-benzyl-1,4-dihydronicotinamide (BNAH) or 1,3-dimethyl-2-phenyl-2,3-dihydro-1*H*-benzo[*d*]imidazole (BIH) as sacrificial electron donors under visible light irradiation (λ > 420 nm). The photochemical reaction is highly selective giving solely formate as carbon containing product (**Figures S21-S23**).[5,37] The additional sacrificial electron donors are required, as the redox potential of TEOA is close to or below the HOMO energy levels of both catalysts (**Figure 2c**), preventing an efficient electron transfer to the chromophore moiety, resulting in a TOF < 0.05 h⁻¹ (**Table S8**). When BIH is used, TOFs of 3.0 h⁻¹ (280

µmol/h/g_cat for 8 h) and 6.0 h⁻¹ (700 µmol/h/g_cat for 8 h) were achieved for **Cp*Rh@PyBpyCMP** and **Cp*Rh@PerBpyCMP**, respectively (**Figure 3a**). The increases of catalytic activity observed when BIH is used rather than BNAH (TOFs ~1.2 h⁻¹) is in line with the known capacity of BIH to be a stronger reductant resulting in an increased thermodynamic driving force as demonstrated by DFT calculations (**Figure 2c**).[1,38] Thus BIH was used in the following as sacrificial electron donor, while TEOA is still required as base, to overcome the thermodynamic limitation of CO_2 reduction[39] and to deprotonate the oxidized BIH, which then acts as a two electron donor.[1]

As the Cp*Rh-based catalytic centre can be considered to be the same in both materials (see also DFT calculations above), the higher activity of the **PerBpyCMP**-based catalyst might be attributed to its increased capability to absorb light in the visible part (**Figure 1e**).[23] The apparent quantum efficiency (*AQE*),[40] determined in the region of visible light between 420 and 700 nm, increases from ~0.5 % for **Cp*Rh@PyBpyCMP** to ~1 % for **Cp*Rh@PerBpyCMP** (**Figure 3a**, **Table S8**). These values are in line with reported *AQE* data for other heterogeneous photocatalytic CO_2 reduction systems containing metal-based dyes (**Table S9**, for further discussions see SI).[41]

To assess the importance of tethering together the photosensitizer and the catalyst and to construct a fully heterogeneous photosystem, we compared **Cp*Rh@PerBpyCMP** to homogeneous and bi-molecular photosystems (**Table 1** and **Scheme S2**). The highest catalytic activity was indeed achieved using **Cp*Rh@PerBpyCMP**, reaching a TOF of 6 h⁻¹. This superior catalytic activity is most likely linked to a more extended process of quenching of the excited state and electron transport in the fully heterogeneous photosystems than in the homogeneous and bi-molecular photosystems.

To study the benefit of the two fully heterogeneous photosystems on the long-term stability, we compared them to the most active literature known CO_2-to-formate heterogeneous
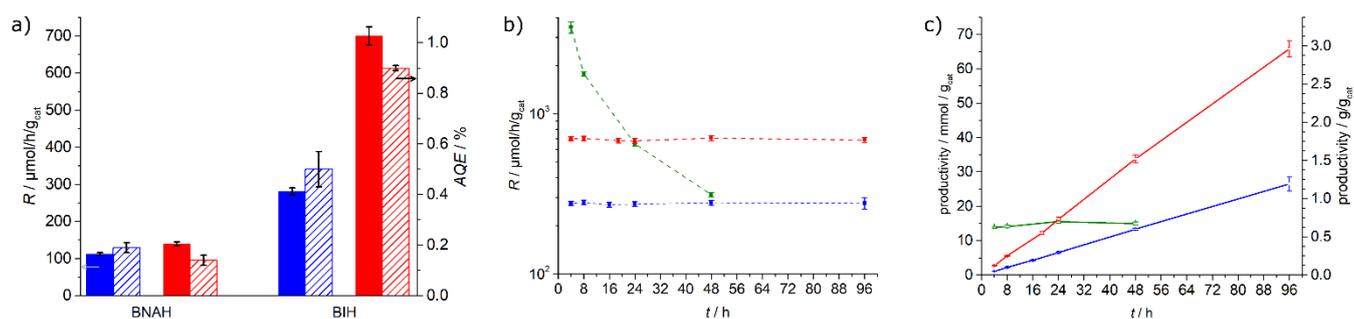
Figure 3. **a)** Comparison of production rate R (left axis, filled columns) and apparent quantum efficiency AQE (right axis, dashed columns) using BNAH or BIH as sacrificial electron donor for **Cp*Rh@PyBpyCMP** (blue) and **Cp*Rh@PerBpyCMP** (red) for 8 h of photocatalysis (~0.9 mM photosensitizer, ~0.05 mM Cp*Rh). **b)** Evolution of production rate for up to 96 h of continuous photocatalysis and **c)** of total productivity in photocatalytic CO_2 reduction of **Cp*Rh@PyBpyCMP** (blue) and **Cp*Rh@PerBpyCMP** (red) as fully heterogeneous photosystems (~0.9 mM photosensitizer, ~0.05 mM Cp*Rh) compared to a photosystem where only the catalyst is heterogenized, here **Cp*Rh@BpyMP-1**[5] and used in the presence of the external molecular photosensitizer $Ru(bpy)_3Cl_2$ (green, up to 48 h, 1 mM $Ru(bpy)_3Cl_2$, ~0.1 mM Cp*Rh. The higher Rh concentration in BpyMP-1 photosystem did not affect its productivity as demonstrated recently.[5]).
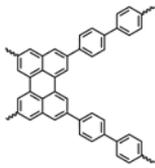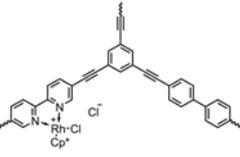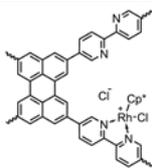
catalysts having the same Cp*Rh-site but without an embedded photosensitizing moiety (*viz.* **Cp*Rh@BpyMP-1**, **Scheme S2**).[5] The **Cp*Rh@BpyMP-1** system therefore requires an external photosensitizer (here 1 mM $Ru(bpy)_3Cl_2$). In case of the bi-molecular **Cp*Rh@BpyMP-1** photosystem, the production rate remains constant for up to 4 h,[5] but a sharp decrease in catalytic activity is observed after more than 4 h (**Figure 3b**). The observed deactivation of $Ru(bpy)_3$-containing photosystem is in line with literature, reporting a loss of activity after 5 to 10 h even for heterogenized systems within various MOFs such as MIL-101 or MOF-253 (see also Table S9).[37,42,43] In contrast, the fully heterogeneous photosystems presented here, which circumvent the need for external $Ru(bpy)_3^{2+}$, are exceptionally photo-stable. To highlight their durability, reactions were performed for up to 96 h of continuous illumination using **Cp*Rh@PerBpyCMP**. No change of the catalytic activity is observed over the course of the reaction, giving rise to TONs of 140 (680 µmol/h/g_{cat}) and 560 (690 µmol/h/g_{cat}) after 24 and 96 h, respectively (**Figure 3b**). Moreover, no observable sign for degradation of the structure or the optical properties could be detected after catalysis (see SI). Regarding the stability of the Rh-based catalytic centres, ICP-OES analysis of the supernatant confirms that no quantifiable leaching of Rh occurs (< 1 ppm). To the best of our knowledge, such a long-term activity has never been achieved so far for photocatalytic CO_2 reduction. We note that also for **Cp*Rh@PyBpyCMP** a constant, albeit lower, production rate was observed for long-term experiments (280 µmol/h/g_{cat}, **Figure 3b** and **Table S8**) without any sign for degradation. As shown in **Figure 2c**, the lower initial activity of the fully heterogeneous photocatalysts **Cp*Rh@PerBpyCMP** and **Cp*Rh@PyBpyCMP** as compared to that of the $Ru(bpy)_3Cl_2$/**Cp*Rh@BpyMP-1** photosystem is clearly exceeded by their remarkable stability for the continuous production of formate, achieving a total productivity up to 3 $g_{formate}$/g_{cat} after four days.

In order to unravel (i) the nature of photo-excited states and (ii) the subsequent electron transfer pathways at the origin of the catalytic activities observed, we performed (i) steady-state emission spectroscopy and (ii) time-correlated single photon counting. These measurements were performed under the conditions of photocatalysis on suspensions of the materials in the acetonitrile-triethanolamine mixture (SI sections 3.6 - 3.8).

Steady-state emission spectroscopy allows to study the relaxation pathways in both photosystems. After light absorption, the photo-excited electrons populate local excited as well as charge-separated states in both materials (**Figure 4a**, **b**). The steady-state emission spectra highlight an important

Table 1. Comparison of fully heterogeneous photosystem **Cp*Rh@PerBpyCMP** with perylene-based bi-molecular photosystems.[a]

Catalyst	Photosensitizer	TOF / h^{-1} [b]
(bpy)Cp*RhCl$_2$	perylene	4.5 ± 0.4
(bpy)Cp*RhCl$_2$	**PerBpCMP**	2.4 ± 0.7
Cp*Rh@BpyMP-1	perylene	1.2 ± 0.1
Cp*Rh@PerBpyCMP		6.0 ± 0.2

[a] 0.18 – 0.23 µmol Rh, 0.1 mM BIH in ACN/TEOA (5/1, V/V), 2 – 4 h. See also **Table S8**, entries 10, 24, 26 and 27. [b] TOF defined as $\frac{n(\text{formate})}{n_{Rh} \cdot t}$
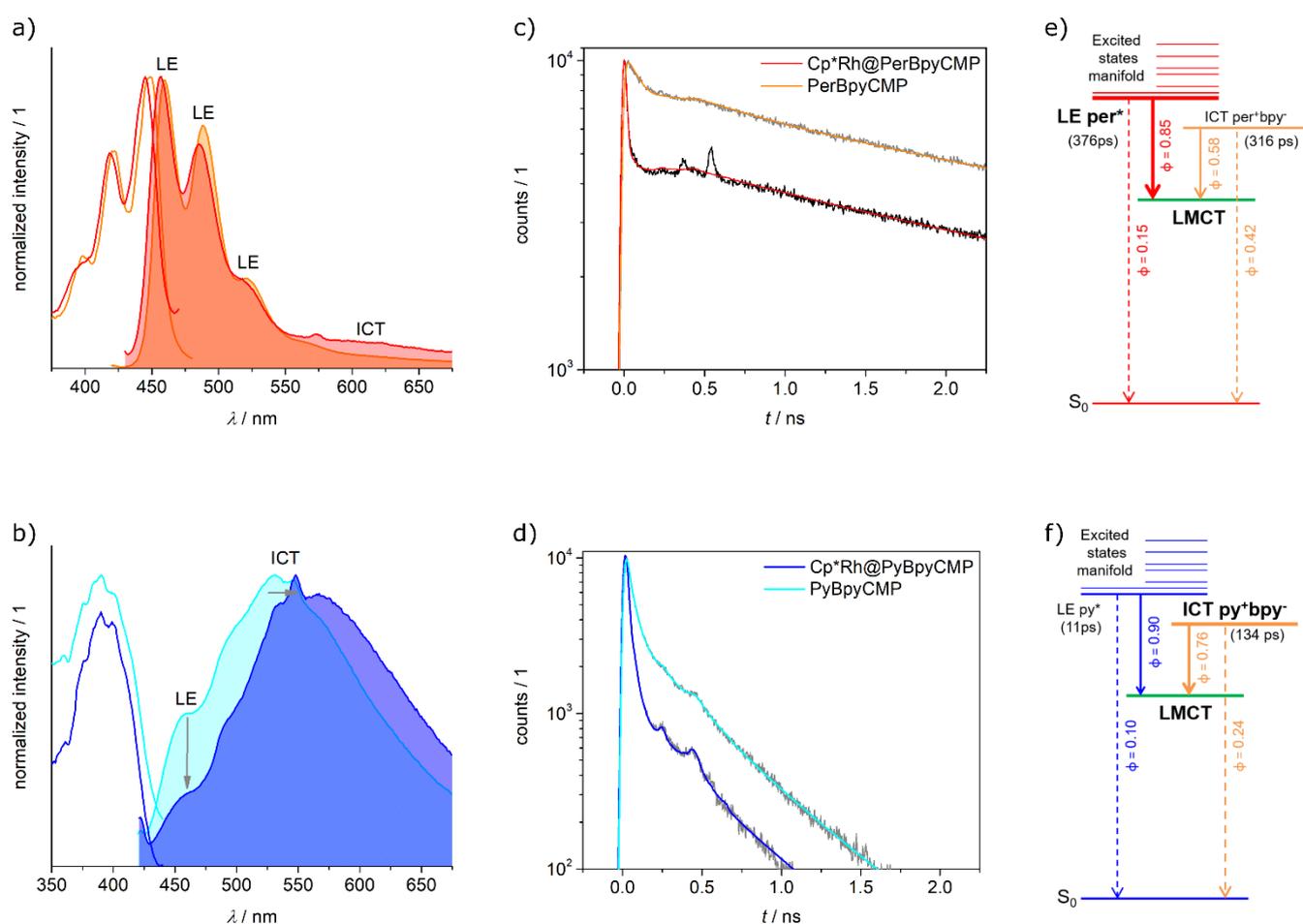
Figure 4. Emission (λ_{ex} = 400 nm) and excitation spectra (λ_{em} = 460 nm) for **a) PerBpyCMP** (orange) and **Cp*Rh@PerBpyCMP** (red) and **b)** emission (λ_{ex} = 400 nm) and excitation spectra (λ_{em} = 488 nm) for **PyBpyCMP** (pale blue) and **Cp*Rh@PyBpyCMP** (blue). TCSPC decays recorded at emission wavelength of the local excited state after excitation at 400 nm **c)** for **PerBpyCMP** (orange) and **Cp*Rh@PerBpyCMP** (red) and **d)** for **PyBpyCMP** (pale blue) and **Cp*Rh@PyBpyCMP** (blue). Schematic representations of electronic energy transfer after photo excitation at 400 nm for **e) Cp*Rh@PerBpyCMP** and **f) Cp*Rh@PyBpyCMP**. Bold arrows represent main transitions, dashed arrows represent side pathways much less likely to occur (quenching efficiencies ϕ are provided and calculated according to SI section 3.8). Note that the time constants for decays of the LMCT-like states are longer than the experimentally accessible time scale.

difference in the population of those photo-excited states between **PerBpyCMP** and **PyBpyCMP** materials, respectively. Elucidating the role of the charge separated states formed upon photoexcitation of conjugated backbones is of great interest to elucidate and optimize the photocatalytic activity of porous materials.[44]

In the case of **Cp*Rh@PerBpyCMP**, and also of the parent **PerBpyCMP**, the spectrum shows the typical vibronic progression of the fluorescence of the perylene molecule (**Figure 4**a).[45,46] Thus, the emission mainly stems from a local excited (LE) state on the perylene moiety (see also the excitation spectra in **Figure 4**a). This point is in good agreement with the calculated HOMO and LUMO which are rather centred on the perylene moiety (**Figure 2**). In clear contrast the steady-state emission spectrum of **Cp*Rh@PyBpyCMP**, as well as the spectrum of the parent **PyBpyCMP**, exhibit a broad and featureless band with a maximum at 520 nm and a secondary weak peak around 450 nm (**Figure 4b**).[47] The major contribution is attributed to an

ICT state in the form of (Py$^+$Bpy$^-$)* associated with a broad excitation spectrum extending from the near UV to 500 nm and featuring a maximum at 520 nm (**Figure 4b**). This ICT involves a charge delocalization from the pyrene toward the bipyridine moiety,[48–50] and represents a stabilization of the photo-generated electron on the polymers backbone,[34,51] in line with the calculated LUMO for [py$_2$(bpy)] (see **Figure 2a**). To sum-up, after photoexcitation and subsequent vibrational relaxation the photo-excited electron populates different states in both materials. In **PerBpyCMP**-based materials, the photo-excited electron occupies mostly a local excited state centred on the perylene moiety (**Figure 2a**), whereas in **PyBpyCMP**-based materials it is delocalized between bipyridine and pyrene orbitals (**Figure 2a**), populating in an internal charge transfer state.

To understand which pathway is more favoured in the activation of the catalytic Rh-centre, the emission lifetimes of the different excited states were characterized by time-correlated single-photon counting (TCSPC). For both catalysts, the

analysis of the TCSPC decays reveals that in the presence of Cp*Rh, a new reactive pathway is opened compared to pristine polymers, resulting in an efficient quenching of the emittive states (**Figure 4c**, **d** and **Table S3**, **S6**). Notably, the mean decay time for the LE state is strongly reduced from 110 ps (**PyBpyCMP**) to less than 11 ps (**Cp*Rh@PyBpyCMP**), and from 2300 ps (**PerBpyCMP**) to 376 ps (**Cp*Rh@PerBpyCMP**). The lifetimes of the ICT contributions are also reduced in **Cp*Rh@PyBpyCMP** and **Cp*Rh@PyBpyCMP** as compared to the pristine polymers. Those findings are in good agreement with the calculated electronic structure of the lowest excited state of **Cp*Rh@PyBpyCMP** and **Cp*Rh@PyBpyCMP** (**Figure 2**) exhibiting a strong LMCT character that results from the localisation of the electron on the bipyridine moiety close to the metal centre, whereas for the non-complexed bipyridine, the excitation is localized on the chromophore moiety (pyrene or perylene, respectively). Therefore, our time-resolved emission measurements firmly establish the efficient quenching of the excited states of the chromophores to form a LMCT-like state with the electron localized close to the metal centre.[24,49,50,52,53] Indeed, the high quenching efficiencies for the LE states of up to 90 % are particularly remarkable because the Rh:chromophore ratio of only 1:20 in the solids necessarily implies long range interactions. In comparison to the LE state, the ICT states observed in both photosystems are less efficiently quenched (**Figure 4e**, **f** and **Table S6**). These results suggest that the formation of ICT states reduces the yield of activation of the LMCT state. The exact proportion of LE and ICT states is still a matter of investigation. However, the efficient electron transfer from LE states directly to the LMCT-like state, that can be further stabilized as a long-lived triplet state,[48–50] is key to drive the photochemical reduction reaction, as the charge separation electron will be located on the catalytically active bipyridine-Rh moiety.[1,34,35]

Thus, this combined spectroscopic study demonstrates that the higher productivity of **Cp*Rh@PerBpyCMP** correlates with its higher capability to absorb visible light (**Figure 1e**) in addition to the favoured formation of local excited states and a more efficient photo-induced electron transfer (quenching) from the local excited state of the organic chromophore towards the catalytically active centre.

Conclusion

In summary, we have demonstrated that the 3-dimensional structuration of the two partners of a photosystem allows for a perfect interplay between active sites at the origin of its superior efficiency. The direct tethering of light harvesting (pyrene or perylene chromophores) and catalytically active sites (Cp*Rh) into conjugated porous polymers allow for an efficient and ultrafast electronic energy transfer, correlating with the catalytic activity, as anticipated by DFT calculations and evidenced by time-resolved spectroscopy. The calculations showed that the chromophores indeed control the HOMO electronic level, while the LUMO is metal-centred. This unique structuration of a long-term stable perylene photosensitizer and a selective Rh-based catalyst into

Cp*Rh@PerBpyCMP renders the photoreduction of CO_2 to formate possible with constant performances over several days under visible light irradiation. The formate production with **Cp*Rh@PerBpyCMP** around 65 mmol/g_{cat} (*i.e.* 3 $g_{formate}$/g_{cat}, after four days) is the highest obtained so far in heterogeneous photocatalysis. Furthermore, the detailed insights into electron transport processes open new perspectives for further optimization and design of photoactive polymers taking advantage of their high synthetic versatility and guided by a computational screening at the molecular level.

[1] Y. Yamazaki, H. Takeda, O. Ishitani, *J. Photochem. Photobiol. C Photochem. Rev.* **2015**, *25*, 106–137.
[2] N. Elgrishi, M. B. Chambers, X. Wang, M. Fontecave, *Chem. Soc. Rev.* **2017**, *46*, 761–796.
[3] Y. H. Luo, L. Z. Dong, J. Liu, S. L. Li, Y. Q. Lan, *Coord. Chem. Rev.* **2019**, *390*, 86–126.
[4] M. Ding, R. W. Flaig, H.-L. Jiang, O. M. Yaghi, *Chem. Soc. Rev.* **2019**, *48*, 2783–2828.
[5] F. M. Wisser, P. Berruyer, L. Cardenas, Y. Mohr, E. A. Quadrelli, A. Lesage, D. Farrusseng, J. Canivet, *ACS Catal.* **2018**, *8*, 1653–1661.
[6] H. Rao, C. Lim, J. Bonin, G. M. Miyake, M. Robert, *J. Am. Chem. Soc.* **2018**, *140*, 17830–17834.
[7] J. Hawecker, J.-M. Lehn, R. Ziessel, *J. Chem. Soc., Chem. Commun.* **1985**, *20*, 56–58.
[8] A. Savateev, M. Antonietti, *ACS Catal.* **2018**, *8*, 9790–9808.
[9] X. B. Li, C. H. Tung, L. Z. Wu, *Nat. Rev. Chem.* **2018**, *2*, 160–173.
[10] A. G. Slater, A. I. Cooper, *Science* **2015**, *348*, aaa8075.
[11] L. Chen, Z. Guo, X. G. Wei, C. Gallenkamp, J. Bonin, E. Anxolabéhère-Mallart, K. C. Lau, T. C. Lau, M. Robert, *J. Am. Chem. Soc.* **2015**, *137*, 10918–10921.
[12] X. Wang, K. Maeda, A. Thomas, K. Takanabe, G. Xin, J. M. Carlsson, K. Domen, M. Antonietti, *Nat. Mater.* **2009**, *8*, 76–80.
[13] G. Zhang, Z.-A. Lan, X. Wang, *Angew. Chem. Int. Ed.* **2016**, *55*, 15712–15727.
[14] L. Wang, Y. Zhang, L. Chen, H. Xu, Y. Xiong, *Adv. Mater.* **2018**, *30*, 1–12.

[15] V. S. Vyas, V. W. H. Lau, B. V. Lotsch, *Chem. Mater.* **2016**, *28*, 5191–5204.

[16] C. Cometto, R. Kuriki, L. Chen, K. Maeda, T. Lau, O. Ishitani, M. Robert, *J. Am. Chem. Soc.* **2018**, *140*, 7437–7440.

[17] N. Chaoui, M. Trunk, R. Dawson, J. Schmidt, A. Thomas, *Chem. Soc. Rev.* **2017**, *46*, 3302–3321.

[18] R. S. Sprick, Y. Bai, C. M. Aitchison, D. J. Woods, A. I. Cooper, **n.d.**, DOI 10.26434/chemrxiv.6217451.v1.

[19] S. Yang, W. Hu, X. Zhang, P. He, B. Pattengale, C. Liu, M. Cendejas, I. Hermans, X. Zhang, J. Zhang, J. Huang, *J. Am. Chem. Soc.* **2018**, *140*, 14614–14618.

[20] P. Huang, J. Huang, S. A. Pantovich, A. D. Carl, T. G. Fenton, C. A. Caputo, R. L. Grimm, A. I. Frenkel, G. Li, *J. Am. Chem. Soc.* **2018**, *140*, 16042–16047.

[21] R. Kuriki, K. Sekizawa, O. Ishitani, K. Maeda, *Angew. Chem. Int. Ed.* **2015**, *54*, 2406–2409.

[22] H. P. Liang, A. Acharjya, D. A. Anito, S. Vogl, T. X. Wang, A. Thomas, B. H. Han, *ACS Catal.* **2019**, *9*, 3959–3968.

[23] M. Sachs, R. S. Sprick, D. Pearce, S. A. J. Hillman, A. Monti, A. A. Y. Guilbert, N. J. Brownbill, S. Dimitrov, X. Shi, F. Blanc, M. A. Zwijnenburg, J. Nelson, J. R. Durrant, A. I. Cooper, *Nat. Commun.* **2018**, *9*, 4968.

[24] Z.-H. Yan, M.-H. Du, J. Liu, S. Jin, C. Wang, G.-L. Zhuang, X.-J. Kong, L.-S. Long, L.-S. Zheng, *Nat. Commun.* **2018**, *9*, 3353.

[25] F. M. Wisser, Y. Mohr, E. A. Quadrelli, D. Farrusseng, J. Canivet, *ChemCatChem* **2018**, *10*, 1778–1782.

[26] F. M. Wisser, Y. Mohr, E. A. Quadrelli, J. Canivet, *ChemCatChem* **2019**, 10.1002/cctc.201902064.

[27] S. Wang, M. Xu, T. Peng, C. Zhang, T. Li, I. Hussain, J. Wang, B. Tan, *Nat. Commun.* **2019**, *10*, 676.

[28] L. Wang, F. S. Xiao, *ChemCatChem* **2014**, *6*, 3048–3052.

[29] L. Li, Z. Cai, Q. Wu, W. Y. Lo, N. Zhang, L. X. Chen, L. Yu, *J. Am. Chem. Soc.* **2016**, *138*, 7681–7686.

[30] M. A. Zwijnenburg, G. Cheng, T. O. McDonald, K. E. Jelfs, J. X. Jiang, S. Ren, T. Hasell, F. Blanc, A. I. Cooper, D. J. Adams, *Macromolecules* **2013**, *46*, 7696–7704.

[31] R. S. Sprick, J.-X. Jiang, B. Bonillo, S. Ren, T. Ratvijitvech, P. Guiglion, M. A. Zwijnenburg, D. J. Adams, A. I. Cooper, *J. Am. Chem. Soc.* **2015**, *137*, 3265–3270.

[32] L. Guo, Y. Niu, S. Razzaque, B. Tan, S. Jin, *ACS Catal.* **2019**, *9*, 9438–9445.

[33] E. C. Constable, M. Neuburger, P. Rösel, G. E. Schneider, J. A. Zampese, C. E. Housecroft, F. Monti, N. Armaroli, R. D. Costa, E. Ortí, *Inorg. Chem.* **2013**, *52*, 885–897.

[34] M. Schulz, M. Karnahl, M. Schwalbe, J. G. Vos, *Coord. Chem. Rev.* **2012**, *256*, 1682–1705.

[35] H. Ozawa, K. Sakai, *Chem. Commun.* **2011**, *47*, 2227–2242.

[36] Y. Bai, L. Wilbraham, B. J. Slater, M. A. Zwijnenburg, R. S. Sprick, A. I. Cooper, *J. Am. Chem. Soc.* **2019**, *141*, 9063–9071.

[37] M. B. Chambers, X. Wang, N. Elgrishi, C. H. Hendon, A. Walsh, J. Bonnefoy, J. Canivet, E. A. Quadrelli, D. Farrusseng, C. Mellot-Draznieks, M. Fontecave, *ChemSusChem* **2015**, *8*, 603–608.

[38] Y. Tamaki, O. Ishitani, *ACS Catal.* **2017**, *7*, 3394–3409.

[39] J. Artz, T. E. Müller, K. Thenert, J. Kleinekorte, R. Meys, A. Sternberg, A. Bardow, W. Leitner, *Chem. Rev.* **2018**, *118*, 434–504.

[40] A. V. Emeline, A. E. Cassano, A. M. Braun, V. N. Parmon, L. Palmisano, S. E. Braslavsky, M. I. Litter, N. Serpone, *Pure Appl. Chem.* **2011**, *83*, 931–1014.

[41] R. Li, W. Zhang, K. Zhou, *Adv. Mater.* **2018**, *30*, 1705512.

[42] T. K. Todorova, T. N. Huan, X. Wang, H. Agarwala, M. Fontecave, *Inorg. Chem.* **2019**, *58*, 6893–6903.

[43] D. Sun, Y. Gao, J. Fu, X. Zeng, Z. Chen, Z. Li, *Chem. Commun.* **2015**, *51*, 2645–2648.

[44] M. Gutierrez, B. Cohen, F. Sánchez, A. Douhal, *Phys. Chem. Chem. Phys.* **2016**, *18*, 27761–27774.

[45] J. R. Lakowicz, *Principles of Fluorescence Spectroscopy*, Springer Science+Business Media, LLC, **n.d.**

[46] O. F. Mohammed, E. Vauthey, *J. Phys. Chem. A* **2008**, *112*, 3823–3830.

[47] A. Philippon, F. Fages, T. Soujanya, M. Vallier, S. Leroy, *J. Phys. Chem. A* **2002**, *104*, 9408–9414.

[48] A. J. Howarth, M. B. Majewski, M. O. Wolf, *Coord. Chem. Rev.* **2015**, *282–283*, 139–149.

[49] D. S. Tyson, F. N. Castellano, *J. Phys. Chem. A* **1999**, *103*, 10955–10960.

[50] A. Harriman, M. Hissler, R. Ziessel, *Phys. Chem. Chem. Phys.* **1999**, *1*, 4203–4211.

[51] Z. Y. Bian, S. M. Chi, L. Li, W. Fu, *Dalt. Trans.* **2010**, *39*, 7884–7887.

[52] R. Ziessel, P. Stachelek, A. Harriman, G. J. Hedley, T. Roland, A. Ruseckas, I. D. W. Samuel, *J. Phys. Chem. A* **2018**, *122*, 4437–4447.

[53] M. Bonchio, Z. Syrgiannis, M. Burian, N. Marino, E. Pizzolato, K. Dirian, F. Rigodanza, G. A. Volpato, G. La Ganga, N. Demitri, S. Berardi, H. Amenitsch, D. M. Guldi, S. Caramori, C. A. Bignozzi, A. Sartorel, M. Prato, *Nat. Chem.* **2019**, *11*, 146–153.